Limitations of Output Power and Efficiency of Simple Resonant-Tunneling-Diode Oscillators

Christian Spudat, Petr Ourednik, Gabriele Picco, Dinh Tuan Nguyen, and Michael Feiginov

***Abstract*—We show that the maximum output power of a simple resonant-tunneling-diode (RTD) oscillator is fundamentally limited by the radiation conductance of its antenna and by a maximum RTD voltage swing. For stand-alone RTD oscillators with common simple antenna types, this power level most likely cannot exceed 1 mW at sub-THz and THz frequencies. The RTD current density, conductance, and capacitance have no direct influence on the maximum power level but those RTD parameters determine how close one can get to the maximum. We show that the maxima of the output power and dc-to-RF conversion efficiency are achieved for different sets of the parameters of RTD oscillators and not simultaneously. We demonstrate slot-antenna RTD oscillators with up to 0.5-mW output power at $\approx$100 GHz and with 5% conversion efficiency, which could be increased further up to 8%, although at the expense of reduced output power. Composite RTD oscillators with separate resonators and radiators can possibly overcome the limitations of simple oscillators.**

***Index Terms*—Efficiency, oscillators, output power, resonant-tunneling diodes (RTDs), THz sources.**

I. Introduction

RESONANT-TUNNELING diodes (RTDs) have a high potential as an enabling technology for real-world sub-THz and THz applications [1], [2]. The operation of RTD oscillators at frequencies up to nearly $\approx$ 2 THz has been demonstrated [3]. However, the power emitted into free space by fundamental-frequency RTD oscillators still remains limited. For stand-alone RTD oscillators, it is significantly below 1 mW [1], [2], [4], [5], [6]. Although an array of RTD oscillators with $\approx$10-mW output power at sub-THz frequencies has been reported recently [6], nevertheless, stand-alone RTD oscillators are the basic building blocks of an array and understanding the limitations of the stand-alone RTD oscillators is of crucial importance for understanding the limitations of the technology and its required complexity level to achieve performance acceptable for applications.

An RTD oscillator consists of a resonator, a radiating antenna (which is often combined with the resonator as a resonant antenna), and an RTD with negative differential conductance (NDC). Each of these components has a complicated internal structure. Therefore, the optimization of the radiated power of RTD oscillators is by far not a trivial task since the oscillator properties are controlled by many parameters with a complicated interplay between them.

We show in this article that one can define a simple framework, allowing for an assessment of the output power, its maximum level, and the efficiency of different RTD oscillators. First, we apply the analysis framework to RTD $I-V$ curves approximated by a third-order polynomial function, and then, we extend the analysis to real (arbitrary) RTD $I-V$ curves. This analysis leads us to conclude that stand-alone RTD oscillators with commonly used simple antennas are unlikely to exceed 1-mW output-power level.

Furthermore, we demonstrate RTD oscillators working close to the maximum of their output power for a given RTD wafer and a simple slot-antenna geometry. The oscillators also demonstrate high dc-to-RF (radio frequency) conversion efficiency.

Manuscript received 9 August 2022; revised 26 October 2022; accepted 2 December 2022. Date of publication 9 December 2022; date of current version 18 January 2023. This work was supported in part by the Austrian Science Fund (FWF) under Grant P30892-N30 and in part by the TU Wien Bibliothek through its Open Access Funding Program. *(Christian Spudat, Petr Ourednik, and Gabriele Picco contributed equally to this work.) (Corresponding author: Michael Feiginov.)*

The authors are with the Department of Electrical Engineering and Information Technology, TU Wien, 1040 Vienna, Austria (e-mail: christian.spudat@tuwien.ac.at; petr.ourednik@tuwien.ac.at; gabriele.picco@tuwien.ac.at; dinh.nguyen@tuwien.ac.at; michael.feiginov@tuwien.ac.at).

Color versions of one or more figures in this article are available at https://doi.org/10.1109/TTHZ.2022.3228069.

Digital Object Identifier 10.1109/TTHZ.2022.3228069

II. Theory

A. Third-Order Approximation for RTD $I-V$ Curve

A third-order approximation for the RTD $I-V$ curve is the lowest-order approximation, which reproduces the shape of the RTD $I-V$ curve with the NDC region and the peak and valley points. It provides a convenient model for a simplified semiquantitative analysis of the nonlinear properties of RTDs and RTD oscillators [8], [9]. We start with this model and approximate the RTD $I-V$ curve as

$$j = g_0 V + b V^3 \tag{1}$$

where j and V are the deviations of the RTD current density and bias from the RTD quiescent (dc) point (j_{dc} and V_{dc}), which we choose at the center of the NDC region, see the red curve in Fig. 1; g_0 is the (static) linear RTD conductance ($g_0 < 0$) and b is the third-order nonlinear coefficient.

Setting the RTD conductance ($g_0 + 3bV^2$) equal to zero, one finds the peak and valley points of the $I-V$ ($j-V$ in this case) curve and the following expressions for the parameters g_0 and b:

$$g_0 = -\frac{3}{2}\frac{\Delta j}{\Delta V} \tag{2}$$

$$b = -\frac{4}{3}\frac{g_0}{\Delta V^2} \tag{3}$$

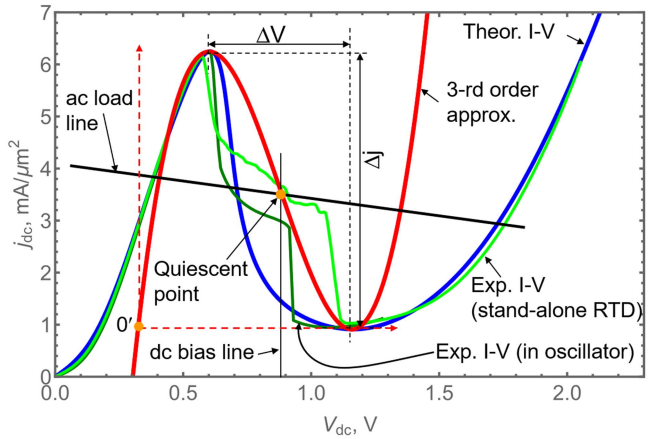

Fig. 1. Red curve shows a third-order approximation matching the peak and valley points of an experimental $I-V$ curve. We sketch the working point at the center of the third-order $I-V$ curve together with the corresponding dc and ac load lines. Blue and green curves show the theoretical and experimental $I-V$ curves, respectively, of an RTD with 1.6-nm barriers studied in [7]. The point $0'$ indicates an idealized position of the current and bias zero point to minimize the dc power of an RTD with a third-order $I-V$ curve.

where Δj and ΔV are the current-density and voltage separations between the peak and valley points, respectively, of an N-shaped RTD $I-V$ curve (see Fig. 1).

Furthermore, one applies a harmonic ac voltage to the RTD ($V = V_{\rm ac}\cos(\omega t)$, where ω is an angular ac frequency) and calculates an ac current density with (1), which also contains higher harmonics due to the nonlinearity of the RTD $I-V$ curve. Selecting the first harmonic, we get the RTD conductance ($g^{(1)}$) at the ac frequency ω:

$$g^{(1)} = g_0 + \frac{3}{4} b\, V_{\rm ac}^2 \tag{4}$$

which is dependent on the ac amplitude ($V_{\rm ac}$). Substituting (3) into (4), we can rewrite the above equation in the form

$$g^{(1)} = g_0 \left(1 - \frac{V_{\rm ac}^2}{\Delta V^2}\frac{1}{\alpha}\right) \tag{5}$$

where α is an additional correction coefficient, introduced here to generalize (5) to the case of an arbitrary RTD I – V curve (see Section II-B), $\alpha = 1$ for a third-order approximation of the $I-V$ curve. Equation (5) shows that $g^{(1)}$ is converging to g_0 for small ac voltages ($V_{\rm ac} \ll \Delta V$), and $|g^{(1)}|$ decreases monotonously to zero at $V_{\rm ac} = \Delta V$ in the case of the third-order approximation.

Furthermore, we include the RTD in a resonator or in a resonant antenna. The oscillator with an RTD could be represented by the equivalent circuit shown in Fig. 2, where A is the RTD area, $c_{\rm RTD}$ is the RTD capacitance per unit area, $G_{\rm r}$ is the antenna radiation conductance, $G_{\rm l}$ represents the Ohmic losses in the antenna ($G_{\rm l} = 0$ in lossless antenna), $Y_{\rm ant}$ is the antenna admittance and its imaginary part ($Im(Y_{\rm ant})$) is the antenna susceptance, which is inductive in typical RTD oscillators; an RTD can have a stray parasitic capacitance ($C_{\rm par}$), its contribution we can combine with $Im(Y_{\rm ant})$, which we denote as $B_{\rm a}$ (the total susceptance of the antenna). An RTD always has contact parasitics, which contain a spreading resistance ($R_{\rm sp}$) and a top-contact resistance ($R_{\rm c}$) with a parallel capacitance ($C_{\rm c}$). In this article, we neglect

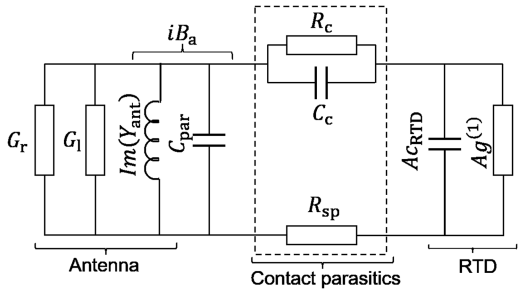

Fig. 2. Equivalent circuit of an RTD oscillator.

contact parasitics based on two reasons. First, we are concerned with the fundamental upper bound for the output power of the RTD oscillators, and the contact parasitics will reduce the maximum output power. Second, in the experimental part of the article, we are dealing with low-frequency ($\sim$100 GHz) RTD oscillators, where the contact parasitics are negligible.

Hence, the oscillation conditions for the RTD could be formulated as follows:

$$\begin{cases} A\, c_{\rm RTD}\, \omega = -B_{\rm a} & (6) \\ -A\, g^{(1)} = G_{\rm r} + G_{\rm l} & (7) \end{cases}$$

where (6) states that the sum of the RTD and antenna/resonator susceptances must be zero at resonance, the equation defines the RTD area (A) for given antenna and frequency. Equation (7) defines the stable oscillation condition when the RTD NDC compensates (exactly) for the total antenna losses ($G_{\rm r} + G_{\rm l}$). This equation defines the RTD oscillation amplitude, since $g^{(1)}$ depends on $V_{\rm ac}$, see (5).

The output power (P) of an RTD oscillator can be written as

$$P = \frac{1}{2} G_{\rm r} V_{\rm ac}^2 \tag{8}$$

Substituting (5) and (7) into (8), we can rewrite it in the form

$$P = \frac{1}{2} G_{\rm r}\, \Delta V^2\, (1-\gamma)\, \alpha \tag{9}$$

with

$$\gamma = \frac{g^{(1)}}{g_0} = -\frac{G_{\rm r} + G_{\rm l}}{g_0\, A}. \tag{10}$$

Note that the parameter γ is positive in the NDC region since $g_0 < 0$. Equation (9) is one of the central equations in this work. Our aim now is to find an upper bound on the output power. We need to consider two cases.

First, we have a given RTD, i.e., $A\, g_0$ is fixed, and have the freedom to adjust the antenna to get a maximum output power. The maximum radiated power will also give the maximum dc-to-RF conversion efficiency (η) of the RTD. Since $A\, g_0 = {\rm const}$ in this case, we can single it out and write (9) and (10) in the form

$$P = \frac{G_{\rm r}}{G_{\rm r} + G_{\rm l}} \frac{1}{2} \Delta V^2 (-g_0\, A)\, \gamma\, (1-\gamma)\, \alpha. \tag{11}$$

For an ideal antenna ($G_{\rm l} = 0$), the first factor will disappear, and P gets a maximum at $\gamma = 1/2$, i.e., $G_{\rm r} = -g_0\, A/2$ for $\alpha = 1$.

This maximum of P (we denote it as P_{ideal}) is equal to

$$P_{\text{ideal}} = \frac{3}{16} A\, \Delta j \Delta V \tag{12}$$

if we replace g_0 with (2). This is a well-known estimate for the output power of an RTD oscillator [8], [9]; it defines the maximum output power extractable out of an RTD with given A and g_0.

However, in a realistic situation, we do not have the freedom to adjust G_{r} arbitrary. In practice, we need to handle the problem of the optimization of the output power of an RTD oscillator from another end. Usually, we have a given RTD wafer with fixed parameters (g_0, b, Δj, ΔV, c_{RTD}). The antenna radiation conductance (G_{r}), its losses (G_{l}), and its total susceptance (B_{a}) can be tuned in certain limits, but these parameters are not independent, they are linked in a well-defined way to each other and to the geometrical parameters of the chosen antenna/resonator type. In practice, we can freely choose only the RTD area A and, in certain limits, the geometrical parameters of the antenna/resonator. Given these limitations, our task is to choose the RTD area and the geometrical antenna parameters to achieve a maximum output power (P). Note, we are looking for a mere maximum of power (P), the conversion efficiency may well turn out to be low or not optimal as the outcome of this procedure.

Therefore, in the second case: We need to find an optimal antenna geometry to maximize (9), where A is a free parameter. The problem can be unraveled rather easily if we note that G_{r} typically grows monotonously towards the eigenfrequency (eigen resonance) of the antenna, when G_{r} takes its maximum value of G_{res}. The power P in (9) should also be growing with G_{r}, unless its growth is damped by the terms with γ in (9). Those terms ($(1-\gamma)$ and α) grow monotonously with a decrease of γ and have maxima at $\gamma = 0$; see discussion on $\alpha(\gamma)$ in Section II-B. Then the upper bound on the output power (P_{max}) of an RTD oscillator is given by the equation

$$P_{\text{max}} = \frac{1}{2} \Delta V^2 G_{\text{res}} \alpha|_{\gamma \to 0} \tag{13}$$

as it follows from (9). This is a universal fundamental limit for the output power of an RTD oscillator.

One can come to (13) also from (8), noting that P is maximized, when G_{r} and V_{ac} are maximized, i.e., when $G_{\text{r}} \to G_{\text{res}}$ and V_{ac} has a maximum. The latter condition is satisfied, when the ac load line ($j = -V(G_{\text{r}} + G_{\text{l}})/A$) in Fig. 1 is much more horizontal than the NDC part of the RTD *I – V* curve around the working point; this condition is equivalent to the requirement $|g^{(1)}| \ll |g_0|$ or $\gamma \ll 1$, and, in this case, $V_{\text{ac}} \to \Delta V$, if we use a third-order approximation for the *I – V* curve, see (5).

Equation (13) is quite obvious. An RTD could be seen as an ac voltage source with an amplitude limitation on the order of ΔV (or equal to ΔV for a third-order approximation for the $I - V$ curve). Then, the power such a source can deliver is eventually limited solely by the load (by the antenna): The larger G_{res} can get, the more power an RTD oscillator can deliver. On the other hand, (13) is very much surprising as it tells us that the properties of an RTD (its current density, g_0 and c_{RTD}) eventually have no impact on P_{max}: P_{max} is solely determined by the maximum of the (resonant) antenna conductance G_{res} and by the maximum RTD voltage swing, which is equal to ΔV for the third-order RTD *I – V* curves. The high current density of an RTD, high g_0, and low c_{RTD} matter for the oscillator output power only to the extent that they allow one to reduce γ when the antenna is operated close to its eigenfrequency. Indeed, according to the second identity in (10), γ decreases with the increase of g_0 and A; the latter growing with the decrease of c_{RTD}, since A is $\propto 1/c_{\text{RTD}}$, see (6).

TABLE I
ASSESSMENTS OF P_{MAX}, ASSUMING $\Delta V = 0.55$ V

Antenna type	R_{res}	G_{res}	P_{max}
	Ω	**mS**	**mW**
$\lambda/2$ slot on a membrane	500	2	0.3
$\lambda/2$ slot on Si	140	7.1	1.1
asymmetric slot on Si	100*	10*	1.5*
square $\lambda/2$ patch	250	4	0.6
wide patch ($\lambda/2 \times 1.75\lambda/2$)	120	8.3	1.2

$R_{\text{res}} = 1/G_{\text{res}}$ is the antenna radiation resistance at resonance.
* Distortion to a single-lobe radiation pattern.

We note P_{max} is not achievable in practice, since to increase G_{r}, we need to increase the antenna dimensions, so that the oscillator operates closer to the eigenfrequency of its antenna; in this case, $B_{\text{a}} \to 0$ and, therefore, $A \to 0$ and γ is diverging ($\gamma \to \infty$), see (6) and (10). Nevertheless, (13) together with (9) and (10) define the basic design strategy, how one can get close to P_{max} for a given antenna type: 1) the antenna should be operated close to its eigen-resonance frequency so that $G_{\text{r}} \to G_{\text{res}}$ (A should be made as small as possible); 2) $\gamma \to 0$, that is achieved by increasing g_0 (and RTD peak current).

The assessments for P_{max} according to (13) for different antenna types are shown in Table I, assuming a rather typical value of 0.55 V for ΔV (this value also corresponds to ΔV of the RTDs discussed in Section III). P_{max} scales quadratically with ΔV. The values of P_{max} in Table I are surprisingly low since G_{res} remains quite low for the most common antenna types used in the RTD oscillators. Specifically:

Symmetric slots: In terms of higher P_{max}, the membrane $\lambda/2$ slots turn out to be inferior to the common slot antennas on InP substrate with Si lens, since they have lower radiation conductance. Additionally, the membrane slots emit equally to both sides of the membrane. Therefore, only half of their P_{max} is usable in practice. The slots on the substrates with a high dielectric constant, on the contrary, emit almost all their radiation into the substrate; hence, almost all their emitted power can be used. Nevertheless, P_{max} for slot antennas on Si turns out to be rather limited and cannot exceed 1 mW in practice.

To get P_{max} of slot-antenna RTD oscillators beyond the limitations of the above basic antenna types, one needs to increase G_{res}. This could be done by using the double-antenna configurations of RTD oscillators, where the slots are coupled to an additional radiator, which could be a broad-band (e.g., Vivaldi [10], [11] or bow-tie [12]) or a resonant [13], [14] antenna. Such oscillators, in principle, can deliver higher output powers.

Asymmetric slots: The concept of asymmetric-slot RTD oscillators has been put forward as a means to increase the output power of the slot-antenna RTD oscillators [5]. Indeed, the asymmetric slots allow one to decouple and separately optimize

the resonator (B_a of the shorter slot arm) and the radiator (G_r of the longer arm) parts of an asymmetric slot. Limitations on G_r of such antennas could be estimated considering a full λ slot with the port at its quarter length, i.e., the radiator arm is $(3/4)\lambda$ long; $G_{res} = 10$ mS in this case. However, the radiation pattern of such antennas might become distorted (the main lobe is deviating from the normal direction to the chip surface) and not have a single-lobe shape (when the radiator length is larger than $\lambda/2$, more lobes appear for longer antennas); e.g., the radiator part was a factor of ≈ 1.2 longer than $\lambda/2$ in the 420-μW RTD oscillator at 548 GHz with an asymmetric slot antenna [5].

Patch antenna: In a typical configuration of the patch RTD oscillators, the patch is connected to a single RTD at the patch edge [15] or to two RTDs [7], [16] at the opposite edges. A wide patch antenna has approximately twice smaller G_{res} compared to that of a $\lambda/2$ square patch antenna. These configurations have G_{res} and P_{max} comparable to that of slot antennas on Si; therefore, P_{max} should also remain limited by ≈ 1 mW. A possibility to get beyond this limit could be realized by shifting the RTDs closer to the center of the patch while keeping the patch length close to $\lambda/2$, which would lead to higher G_{res} and, correspondingly, to higher P_{max}. This method to increase the output power has been demonstrated recently [6], leading to $P \approx 300\,\mu$W at 450 GHz.

Another important parameter for RTD oscillators is the dc-to-RF conversion efficiency (η), which we define as

$$\eta = \frac{P}{A\,p_{dc}} \tag{14}$$

where p_{dc} is the dc power absorbed by RTD per unit area. Substituting (9) and (10) into the above equation, we can rewrite it in the form

$$\eta = \frac{G_r}{G_r + G_l}\beta\gamma\,(1-\gamma)\,\alpha \tag{15}$$

where the constant β is defined as

$$\beta = \frac{-g_0 \Delta V^2}{2p_{dc}}. \tag{16}$$

Both g_0 and p_{dc} are linearly proportional to the RTD peak current density. That makes the constant β independent of the RTD current density, it is determined solely by the (normalized) $I-V$ curve shape; i.e., β is a fixed parameter for a given RTD wafer, and also, it remains the same for different wafers with different current density, but with identical (normalized) $I-V$ curve shape. Thus, for a given $I-V$ curve shape, η can be maximized only by adjusting γ and antenna parameters (by an appropriate change of the RTD current density, g_0, A, G_r, and G_l). That is discussed in Section II-C.

It is instructive to estimate the maximum of the parameter η in the case of a third-order $I-V$ curve. First, we need to minimize p_{dc}. In a best-case scenario, the valley point of the RTD $I-V$ curve should be at the zero RTD current, and the peak point can be, say, at the bias of $\Delta V/2$. The situation is sketched in Fig. 1 with $0'$ as the zero point. In this case, $p_{dc} = \Delta V \Delta j/2$ and, using (2), we get an estimate for the constant $\beta = 3/2$. Further on, $\alpha = 1$ for a third-order $I-V$ curve, and the first factor in (15) disappears for an ideal antenna ($G_l = 0$). Thus, (15) leads to the following estimate for the maximum efficiency of an RTD oscillator:

$$\eta_{max} = \frac{3}{8} \approx 37\% \tag{17}$$

corresponding to $\gamma = 1/2$. Note that an optimum γ has different values for the maxima of η and P, namely, $\gamma \to 0$ for the maximum power, see (9) and (13).

The above analysis of the output power and efficiency is done for the RTD quiescent point in the center of the NDC region of the third-order $I-V$ curve. If the RTD is biased in another point of the NDC region, then $g^{(1)}$ in (5) is reduced and that eventually leads to lower V_{ac}, P_{max}, and η, i.e., the center of the NDC region is an optimum quiescent point for the third-order $I-V$ curves.

B. Real RTD I – V Curve

The above analysis can be easily generalized to the case of an arbitrary RTD $I-V$ curve. One starts with a quasi-static RTD $I-V$ curve ($j(V)$) around a given dc working (quiescent) point (j_{dc} and V_{dc}) and applies a harmonic ac voltage ($V = V_{ac}\cos(\omega t)$)

$$j = j\,(V_{ac}\cos(\omega t))\,. \tag{18}$$

Further on, one calculates the amplitude of the first harmonic of j; divided by V_{ac}, it gives $g^{(1)}(V_{ac})$, which could be written as

$$g^{(1)} = \frac{2}{\pi}\frac{1}{V_{ac}}\int_0^{\pi} j\,(V_{ac}\cos(\xi))\cos(\xi)\,d\xi. \tag{19}$$

In the small-signal limit, as $V_{ac} \to 0$, $j(t)$ in (18) can be approximated as $g_0 V_{ac}\cos(\omega t)$, then (19) is reduced to $g^{(1)} \to g_0$. That is, $g^{(1)}$ converges to g_0 for small V_{ac} for an arbitrary $I-V$ curve, as it should. Then, $g^{(1)}$ in (19) can be represented in the form of (5) for larger amplitudes, where the parameter $\alpha(V_{ac})$ corrects for the deviation of $g^{(1)}(V_{ac})$ from the quadratic dependence on V_{ac} for the real $I-V$ curve. In the case of the third-order $I-V$ curve approximation: $\alpha = 1$. Getting an expression for V_{ac}^2 from (5) and substituting it into (8), we get the general equation (9).

For an illustration, we apply this procedure to an InGaAs/AlAs RTD with 1.6-nm barriers studied in [7], the same RTD we use in Section III. This RTD wafer has rather common characteristics for RTDs used in the sub-THz and THz range. Fig. 1 shows the theoretical and experimental dc $I-V$ curves of the RTD. The theoretical $I-V$ curve was calculated by self-consistent solution of the Schrödinger and Poisson equations; both curves are in good agreement with each other, as reported before [7]. Fig. 1 also shows a third-order approximation of the $I-V$ curve adjusted so that it matches the peak and valley points of the real $I-V$ curve.

Fig. 3 shows a couple of traces of the first-harmonic RTD conductance ($g^{(1)}$) for different dc biases, $g^{(1)}$ is calculated with (19). $g^{(1)}$ strongly depends on the applied bias (V_{dc}) and $g^{(1)}$ is, generally speaking, a nonmonotonous function of V_{ac} for real RTD $I-V$ curves. To simplify the further analysis, we introduce an envelope function of all these $g^{(1)}$ traces for different dc biases, denoted as g_{max}. It is a monotonous function of V_{ac} (see Fig. 3), and it shows the maximum achievable $g^{(1)}$ for given V_{ac}

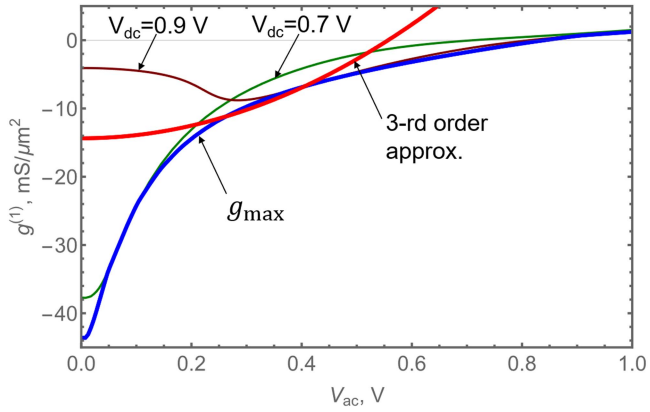

Fig. 3. Thin lines (brown and green) show the dependence of $g^{(1)}$ versus $V_{\rm ac}$ for two dc biases of 0.7 and 0.9 V. The blue line shows the envelope curve ($g_{\rm max}$) for all such traces for different $V_{\rm dc}$. The red curve shows $g^{(1)}$ for a third-order approximation of the $I-V$ curve.

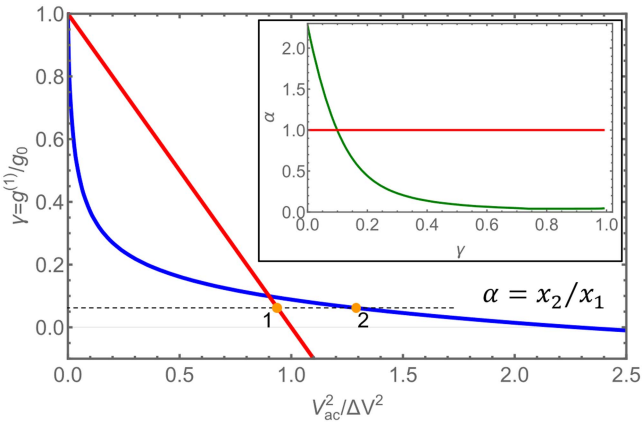

Fig. 4. $g^{(1)}$ (red) and $g_{\rm max}$ (blue) normalized by respective g_0 for a third-order approximation and for a real $I-V$ curve, respectively; these ratios give the parameter γ. The ratio of x coordinates of the two curves at a fixed γ gives the correction parameter α, which can be represented as a function of γ, see inset. The red curve in the inset shows $\alpha=1$ for a third-order approximation.

or, flipping the axis, the maximum achievable amplitude $V_{\rm ac}$ for given $g^{(1)}$, which are the relevant RTD parameters for the power and efficiency optimization of RTD oscillators. Therefore, in the analysis of real RTD I – V curves, under $g^{(1)}(V_{\rm ac})$ we understand $g_{\rm max}(V_{\rm ac})$, and under g_0 in all the above equations, we understand $g_{\rm max}(0)$

$$g^{(1)}(V_{\rm ac}) \to g_{\rm max}(V_{\rm ac}) \tag{20}$$

$$g_0 \to g_{\rm max}(0). \tag{21}$$

Fig. 3 also shows the quadratic (monotonous) curve for $g^{(1)}$ [see (5)] for the case of the third-order approximation of the $I-V$ curve: It has a different g_0 and a different crossing point with the zero axis.

$g_{\rm max}$ and the third-order $g^{(1)}$, being normalized on the respective small-signal conductances (g_0) – which gives the parameter γ – and represented as a function of $V_{\rm ac}^2/\Delta V^2$, are shown in Fig. 4. The ratio of the x-coordinates of the two curves for each

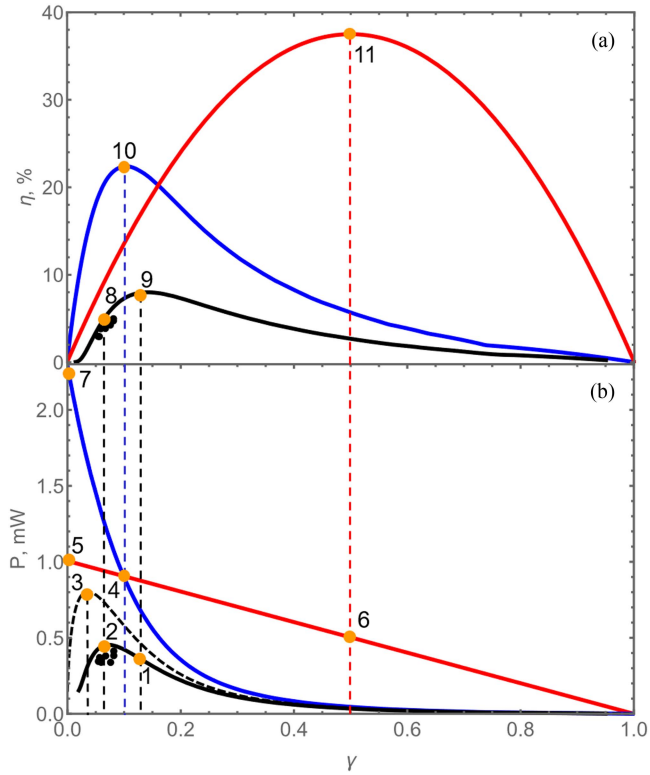

Fig. 5. (a) RTD efficiency and (b) output power as functions of the parameter γ, calculated with (15) and (9). Red lines are calculated for a third-order approximation of the $I-V$ curve ($\alpha=1$), and the blue ones are for a real $I-V$ curve shown in Fig. 1. Those curves in (a) are calculated for an ideal antenna ($G_{\rm l}=0$) and in (b) for an antenna with a maximum of the radiation conductance ($G_{\rm r}=G_{\rm res}$). The black theoretical curves and experimental dots are for an RTD oscillator with 450-μm slot antenna. The dashed line shows the output power for a lossless ($G_{\rm l}=0$) 450-μm antenna, but with an account of $G_{\rm r}<G_{\rm res}$. Different orange points are discussed in the text.

y-coordinate (γ) gives the value of the correction parameter α, which could be represented as a function of γ (see inset in Fig. 4).

The real RTD $I-V$ curve has stronger nonlinearity in the NDC and peak regions than that captured by a third-order approximation, leading to a faster decrease of $g^{(1)}$ with the increase of $V_{\rm ac}$, when $V_{\rm ac} \lesssim \Delta V$, see Figs. 3 and 4. That is also reflected in the low values of the parameter α at $\gamma > 0.2$, see inset in Fig. 4. On the other hand, a weaker nonlinearity of the real RTD $I-V$ curve in the valley region leads to a slower decrease of $g^{(1)}$ at larger $V_{\rm ac}$. Therefore, $V_{\rm ac}$ can overshoot ΔV in the region, where $g^{(1)} \to 0$; that is reflected in $\alpha > 1$ for $\gamma \lesssim 0.1$, see Fig. 4. The parameter α influences P, $P_{\rm max}$, and η, see (9), (13), and (15).

C. Discussion

To illustrate the influence of α on P, $P_{\rm max}$, and η in more detail, we plot η and P as functions of γ in Fig. 5. The red curves correspond to the third-order approximation of the $I-V$ curves ($\alpha=1$), the blue curves in Fig. 5 are for the real $I-V$ curve shown in Fig. 1. Fig. 5(a) shows the curves for these two cases calculated with (15), assuming an ideal antenna ($G_{\rm l}=0$). With the red and blue curves in Fig. 5(b), we plot the maximum power of the RTD oscillator for each γ. The curves

are calculated with (9), assuming that G_r is at its maximum level, i.e., $G_r = G_{res}$. Note, these maximum power levels are not achievable in practice, since $G_r < G_{res}$, yet the curves do define the maximum power level for each γ and the maximum power level does decrease with the increase of γ, i.e., γ has to be made small to achieve a high power level in RTD oscillators. In the limit $\gamma \to 0$, the curves converge to P_{max} given by (13), which are the points 5 and 7 in Fig. 5(b). These curves illustrate several points.

One point is related to the level of P_{max}, which is proportional to $\alpha|_{\gamma\to 0}$, as defined by (13). For the real RTD $I-V$ curve we analyze in this work, $\alpha|_{\gamma\to 0} = 2.3$, i.e., the power at point 7 is 2.3 times higher than that at point 5 for a third-order $I-V$ curve approximation. However, in practice, γ cannot reach 0, P always stays less than P_{max} and $\alpha \approx 1$ for practically usable small values of $\gamma \approx 0.1$ in RTD oscillators. Although we demonstrate experimentally lower values of $\gamma \approx 0.05$ and $\alpha \approx 1.5$ at ≈ 100 GHz in the experimental part of this work (see later), that is rather difficult to do at higher frequencies in the THz range. This example illustrates that the assessments of P_{max} given in Table I for different RTD oscillators hold approximately true for the real (typical) RTD $I-V$ curves.

We note that $P_{max} \approx 1$ mW at point 5 in Fig. 5 is slightly lower than the value given in Table I for an ideal slot antenna on Si. This is due to the fact that we took the value of 6.6 mS for G_{res} in the calculations in Fig. 5. This G_{res} corresponds to 450-μm slot antenna described in the experimental part of the work: G_{res} in a real antenna is slightly reduced by a bridge, finite metal thickness, etc.

The second point is related to the influence of the parameter α on η. In calculating the blue curve in Fig. 5(a), we apply the following procedure. First, we estimate the parameter β with (16). As j_{dc} we take the middle value in the NDC region, which is $\approx 3\,\mathrm{mA}/\mu\mathrm{m}^2$, see Fig. 1; as V_{dc} we take $\approx 0.9\,V$, since the output power of RTD oscillators is usually larger at the right side of the NDC region. That gives an estimate $p_{dc} \approx 2.7\,\mathrm{mW}/\mu\mathrm{m}^2$. Furthermore, we take $g_0 = g_{max}(0)$ as $-44\,\mathrm{mS}/\mu\mathrm{m}^2$, see Fig. 3, and $\Delta V \approx 0.55\,V$. Substituting that in (16), we get an estimate of ≈ 2.5 for the constant β in (15). As a second step, assuming an ideal antenna with $G_l = 0$, we put β and α (see Fig. 4) into (15), the result is shown in Fig. 5(a). Due to larger values of α for lower γ, the maximum of η is shifted to $\gamma \approx 0.1$ and the maximum is reduced to $\approx 22\%$, contrary to $\approx 37\%$ at $\gamma = 0.5$ for the third-order approximation for the $I-V$ curve, compare points 10 and 11 in Fig. 5(a).

The next point relates to the difference in the optima of η and P. For a third-order approximation for the $I-V$ curve, the maximum of η is achieved at $\gamma = 0.5$ (point 11 in Fig. 5). However, the power corresponding to this point (point 6) is twice less than P_{max}, which is achieved at $\gamma = 0$ (point 5), see (9). The situation is similar for a real $I-V$ curve: The maximum of η is achieved at the point 10 for $\gamma \approx 0.1$, corresponding to the power at point 4 (the point is on the blue curve, crossing with the red curve is a coincidence), which is a factor of ≈ 3 lower than P_{max} at point 7.

To illustrate the situation in the real RTD oscillators, we show black curves in Fig. 5, which correspond to the RTD oscillators we studied in the experimental part of the article with a fixed slot antenna of 450-μm length, where γ is changed by sweeping the RTD area A. These curves take into account the real values of G_r and G_l for each γ [those values are linked to γ by the oscillation conditions (6) and (7)], calculation details are explained in the experimental part of the article. In the limit $\gamma \to 0$, A grows and that drives $G_r \to 0$; therefore, the output power $P \to 0$ and $\eta \to 0$ in this limit. Note, these curves for the real RTD oscillators also show that the maxima of the output power and η do not coincide: The maximum of the output power is achieved in point 2, which gives approximately twice smaller η (point 8) compared to a maximum for these oscillators (point 9); on the other hand, for γ corresponding to the maximum of η (point 9), the output power is below the maximum (point 1). The dashed line in Fig. 5(b) shows the output power for an ideal antenna ($G_l = 0$), which would give a higher output power (compare points 2 and 3). The black dots in Fig. 5 correspond to the experimentally measured devices with the parameters close to the maximum of power, but with η below the maximum (see the experimental part of the article).

The procedure described in this article for the assessment of P_{max} and efficiency is based on the analysis of the static RTD $I-V$ curves. The procedure is applicable when RTDs are operating at relatively low frequencies in the quasi-static regime ($\omega\tau_{rel} \ll 1$, where τ_{rel} is the charge-relaxation time constant [17], [18], [19]), although in terms of the absolute frequencies, the RTDs with thin barriers ($\approx$1 nm) work in the quasi-static regime even at frequencies above 1 THz [20]. However, the procedure could also be directly applied to RTDs operating in the high-frequency regime ($\omega\tau_{rel} \gtrsim 1$) but one should use the high-frequency RTD $I-V$ curves in the analysis in this case, rather than the static ones. Contrary to directly measurable static $I-V$ curves, the measurement of the nonlinear high-frequency $I-V$ curves is very complicated; at THz frequencies, such direct measurements are hardly possible. Therefore, in practice, one should rely on the simulated high-frequency RTD characteristics [21]. It is important to note, though, that due to the suppression of the Coulomb interaction, ΔV in the high-frequency regime ($\omega\tau_{rel} \gg 1$) is larger than ΔV for the static $I-V$ curves [21], which can potentially lead to higher P_{max}. However, g_0 is smaller at the high frequencies [17], [18], [19], [21], [22]; therefore, higher P might be difficult to achieve in practice.

Our theoretical discussion in this article focuses on simple RTD oscillators consisting of an RTD and a resonant antenna. However, the presented analysis framework and the stated limitation on the output power (13) are also directly applicable to other or more complex types of RTD oscillators. For example, in the case of coplanar-waveguide (CPW) resonators with CPW output, the equivalent circuit in Fig. 2 remains applicable if we replace G_r with the output-CPW conductance and take it as G_{res}. Since the CPW conductance can be higher than that of simple resonant antennas, P_{max} can exceed the values stated in Table I, as it was demonstrated in [23], although outcoupling of the radiation to the free space from a CPW output can cause additional losses. Also, the composite RTD oscillators, containing separate resonators and radiators [11], [24], could be

represented in the form of the equivalent circuit in Fig. 2, if we take the combined admittance of the resonator and radiator (as "seen" from the RTD port) as Y_{ant}. In this case, G_{r} represents a radiating part of the combined admittance, which could be deemed as the radiator/antenna conductance transformed by the resonator to the RTD port. In other words, the resonator can be regarded as an impedance-matching network, transforming the actual radiator/antenna admittance to the RTD port. As G_{res} in (13) one can take a maximum of G_{r} in the operation range of the oscillator, (G_{r} has a complicated multiresonance frequency dependence in such structures). That leads to higher estimates for G_{res} and P_{max} in complex RTD oscillators compared to the numbers listed in Table I. If the additional losses in the resonators and fabrication complexity of such structures could be surmounted, such composite RTD oscillators are expected to overcome the performance limitations of simple RTD oscillators [24].

Apart from G_{res}, P_{max} is also limited by ΔV. In the analysis of P_{max}, we have assumed $\Delta V = 0.55$ V. This value is typical (or rather at the high end) for RTDs operating at sub-THz and THz frequencies. There might be some room for an increase of ΔV by optimization of the RTD layers but it is unclear how much. For example, the incorporation of a large spacer in the RTD collector [25] leads to an increase of ΔV but that also increases the electron transport time through the collector region, which can prevent the operation of such RTDs at THz frequencies. Additionally, a large collector spacer decreases the RTD conductance, which should lead to an increase of γ and, as a consequence, to the reduction of P.

III. Experiment

In the experimental part of this article, we illustrate that RTD oscillators can be operated in the regime $\gamma \ll 1$ and that an output power close to a maximum (which is below P_{max} due to antenna losses and limited g_0) for a given wafer, given antenna type, and at a given frequency could be achieved. To keep the parameter γ small, we choose relatively low frequencies of ≈ 100 GHz for the RTD oscillators. In this case, RTDs with rather large areas ($> 1\,\mu\text{m}^2$, for the ease of fabrication) can provide small γ.

A. Fabrication

In this work, we are using InGaAs/AlAs RTDs on InP substrate with relatively thick 1.6-nm AlAs barriers sandwiching a composite $In_{0.53}Ga_{0.47}As/InAs/In_{0.53}Ga_{0.47}As$ quantum well (QW) with the nominal thickness of each sublayer of 1.2 nm. The barriers are surrounded by $In_{0.53}Ga_{0.47}As$ layers, which are n-doped at the level of $1.5 \cdot 10^{18}$ cm^{-3} except for 1.2-nm undoped spacers immediately next to the barriers. The more distant n++ $In_{0.53}Ga_{0.47}As$ layers were doped at the level of nominally $5 \cdot 10^{19}$ cm^{-3}. The RTDs have a relatively low peak current density of $\approx 6\,\text{mA}/\mu\text{m}^2$, and the RTD exhibits a peak-to-valley current ratio of ≈ 9. The measured and simulated $I - V$ curves of the RTDs are shown in Fig. 1. Details on these RTDs are presented in [7].

Our RTD oscillators are based on symmetrical slot-antenna resonators mounted on a hemispherical Si lens (underneath the InP substrate). The slot antennas had a nominal width of 4 μm and lengths of 450 μm, 400 μm, 375 μm, and 350 μm. In each antenna, the RTDs had mesa areas in the range 2–5 μm^2. The metallization around the slot antenna contains metal–insulator–metal (MIM) layers on one side of the slot, see schematic in Fig. 6. MIM works as a short circuit at the operating frequencies of the RTD oscillators. Still, it provides two contacts to apply bias to the RTDs. The upper metal layer of the MIM is connected via a bridge to the upper RTD contact. Outside the antenna area, the RTD oscillators contain a shunt resistor to stabilize RTDs at low (quasi-dc) frequencies.

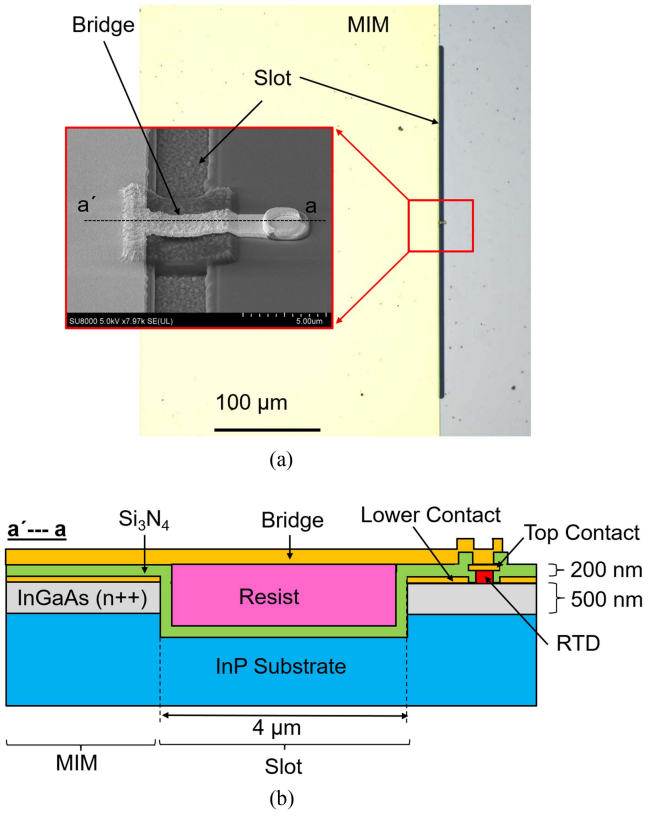

Fig. 6. (a) Optical microscope image of an RTD oscillator with a 350-μm slot antenna. The inset shows a magnified SEM picture of the slot's central area. (b) Schematic of the "a ′— a" cross section containing the RTD mesa, RTD contacts, bridge, and MIM.

Our fabrication process is similar to the one described in the literature [9], with the main difference that we use only optical lithography. We start with the deposition of the top RTD-contact metallization on the RTD wafer, the metallization is Ti/Pd/Au (20/20/250 nm) and its patterning defines the RTD mesa areas. Then, the RTD mesas are wet etched down to n++ InGaAs layer underneath the RTD barriers. As a next step, Ti/Pd/Au (20/20/40 nm) is deposited as the lower RTD contact metallization, and this metallization layer is left open in the slot regions of the antenna. n++ layers are etched subsequently away in the slot. After that, the whole structure is covered by 200 nm of Si_3N_4, which serves as a passivation layer for the RTDs and as an insulator in MIM. Then, the slot was filled with patterned photoresist, and the next metallization layer (Ti/Au, 10/250 nm)

was deposited as the top MIM layer and the bridge to the RTD mesas. As the final step, we deposited indium tin oxide (ITO) shunt resistors.

B. Measurements of RTD Oscillators

The spectra of the emitted radiation of the RTD oscillators were measured with a Martin–Puplett interferometer, designed to cover the frequencies from 50 GHz to 5 THz. The frequency resolution of the interferometer is ≈ 1 GHz. As a radiation detector, we have been using a Golay cell.

The output power of the RTD oscillators was measured with a calibrated pyroelectric detector. During power measurements, the detector was mounted right after a hemispherical (3-cm diameter) Si lens. The measured power has been corrected for the back reflection at the surface of the Si lens ($\approx 30\%$) and the overlap of the radiation beam pattern with the clear aperture of the detector (collection efficiency is 30%–50%). The radiation beam pattern for the used slot antennas was calculated for different antennas with a commercial electromagnetic simulator. This procedure has provided us with the data for the output power of RTD oscillators reported below. The dc-to-RF conversion efficiency (η) of the RTDs in the oscillators has been defined as the ratio of the oscillator output power and the dc power consumed by the RTD. The dc losses in shunt have been excluded from this definition for the sake of clarity of comparison with the literature data and since such shunt losses could, in general, be excluded by replacing the shunt with properly designed RC circuits [6], [25].

C. Modeling of RTD Oscillators

In the modeling, an RTD oscillator could be divided into two parts. One part is linear, which includes the antenna/resonator, see Fig. 2. Its frequency-dependent admittance ($iB_\mathrm{a} + G_\mathrm{l} + G_\mathrm{r}$) has been calculated with a commercial electromagnetic simulator for each of the fabricated antennas. This part also contains a parasitic capacitance (C_par) of the RTDs, which is due to an overlap of the bridge with the lower RTD contact layer, see Fig. 6. We estimate C_par to be ≈ 1.2 fF for our devices, and it is included into B_a in the simulation model. The second part is nonlinear, which is the RTD itself. The RTD conductance ($g^{(1)}$) is calculated by averaging its static $I-V$ curve, as described in Section II-B. We can apply this quasi-static calculation procedure to our RTDs, since $\omega\tau_\mathrm{rel}$ for our RTDs is $\ll 1$ at the frequencies of ≈ 100 GHz. The capacitance c_RTD for our RTDs is 9 fF/μm^2.

Knowing B_a and c_RTD, the oscillation frequency is calculated with (6) for each antenna length and each RTD-mesa area. The comparison between the measured and simulated frequencies for different antennas and different RTD areas is shown in Fig. 7. Experimental values for the RTD areas are determined by dividing the total RTD current (without shunt) by the RTD current density. We attribute some scattering in the measured frequencies to nonsystematic deviations of the antenna parameters from the nominal values. Overall agreement with the experiment is at a rather good level.

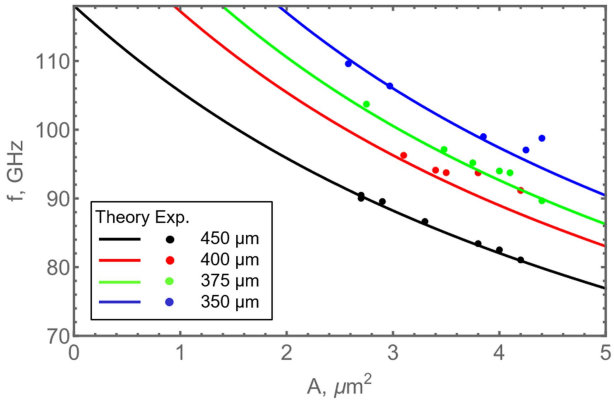

Fig. 7. Oscillation frequency versus RTD area for oscillators with slot-antenna lengths of 450 μm, 400 μm, 375 μm, and 350 μm. Solid lines show theoretical curves and the dots show the experimental points.

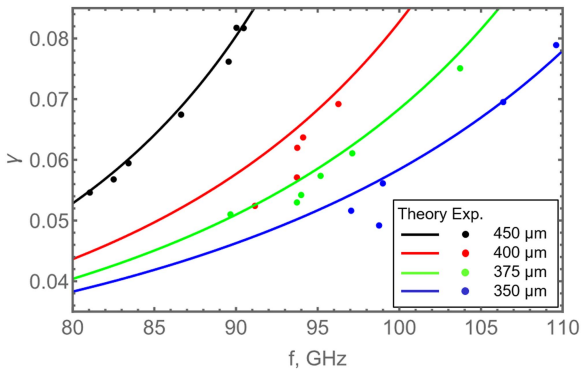

Fig. 8. Plot shows a relation between the parameter γ and frequency for different slot antennas. Solid lines show theoretical curves, the dots show the experimental data points. The parameter γ for the latter ones is calculated with (10) based on the RTD area and simulated values of G_r and G_l at the measured frequency.

Further on, knowing the measured oscillation frequency for each antenna and RTD mesa area, we take the calculated values of $G_\mathrm{l} + G_\mathrm{r}$ at the given frequency for the respective antenna; substituting them into (7), we get the value of $g^{(1)}$. We then substitute it, A, and g_0 into (10) and get the values of γ for each oscillator. For our RTD wafer, $g_0 = -44$ mS/μm^2, as one can see in Fig. 3. Fig. 8 shows the values of γ calculated in such a way for the measured oscillators. Since the frequencies of the oscillators are scattered around the theoretical curves, we see a similar scattering also for the values of γ in Fig. 8 (as a rough estimate, the inaccuracy of the definition of γ is $<10\%$). The theoretical curves in Fig. 8 are also calculated with (10); we sweep A for each antenna, which gives us different frequencies and then A and $G_\mathrm{l} + G_\mathrm{r}$ at the given frequency are put into (10), and that gives us the theoretical curves shown in Fig. 8.

Furthermore, the output power and RTD conversion efficiency were calculated with (9) and (15) as functions of frequency and γ. The results are shown in Figs. 9 and 10. The figures also show the experimental points for the output power and efficiency (η); the corresponding frequencies for these points were directly measured, then – following the above procedure (see Fig. 8) – the parameter γ was calculated for each frequency.

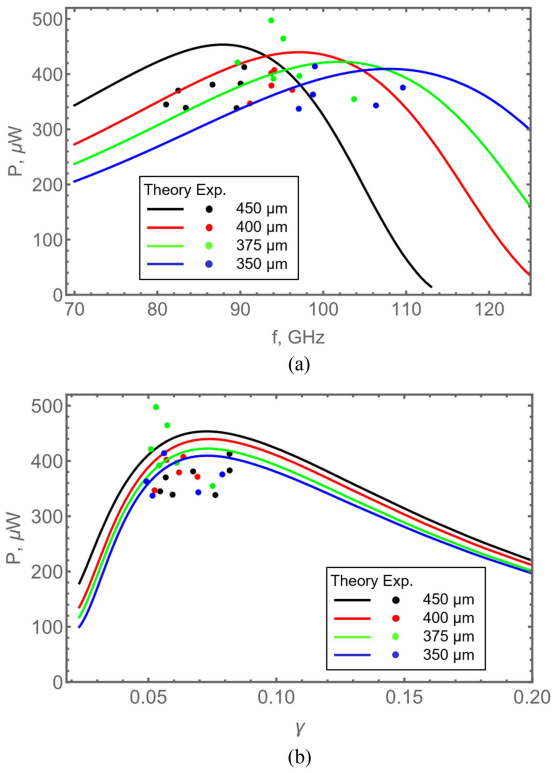

Fig. 9. (a) Theoretical and experimental output power versus frequency for different antennas. (b) Plot shows the same data recalculated as P versus γ.

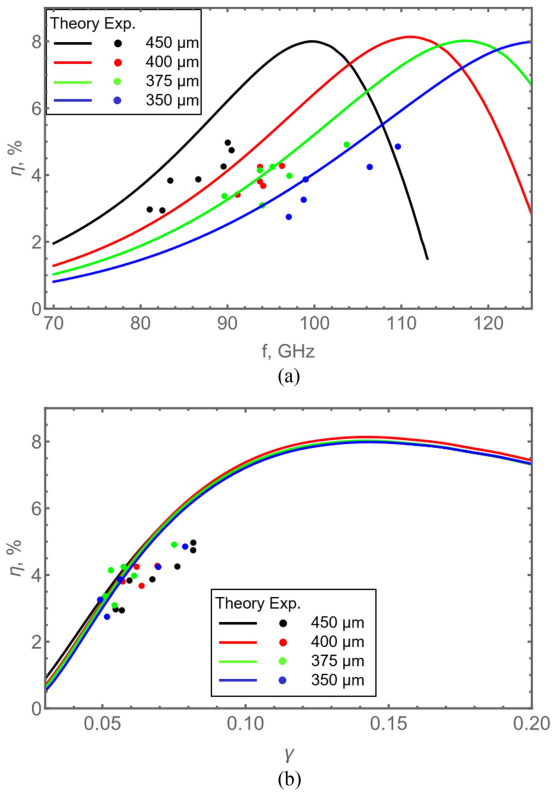

Fig. 10. (a) Theoretical and experimental values of the dc-to-RF conversion efficiency (η) versus frequency for different slot antennas. (b) Plot shows the same data recalculated as η versus γ.

TABLE II
PUBLISHED AND OUR DATA ON STAND-ALONE RTD OSCILLATORS WITH HIGH EFFICIENCY

Ref.	Freq.	Power	J	η
	GHz	μW	mA/μm^2	%
[25]	34	2500	2	14.7†
[21], [26]	109	8	0.23	2.7
[23]	260	1000	3	1†*
[4]	443	200	18	1.1
[6]	450	320	-	1
[5]	548	420	24	1.45
Current work	90	383	6	5.0
	94	500	6	4.1
	110	376	6	4.9

† on-wafer measurements, oscillators without antenna.
* estimate, the data are not explicitly stated in the article.

D. Discussion

Fig. 9(a) shows that the oscillators we experimentally studied worked close to the maximum output power for given antennas. More clearly, one can see that in the plot for power versus γ in Fig. 9(b). The plot shows that the maximum of the power is reached for $\gamma \approx 0.05$–0.08, and the measured oscillators are exactly in this range. Several experimental points are higher than the theoretical curves, and we assume that happened due to some nonsystematic deviations in the antenna dimensions or lower parasitics.

However, Fig. 10(a) shows that the efficiency η, although high, is not at its maximum; it keeps growing with an increase in frequency (with the decrease of A) for our set of devices. Fig. 10(b) shows this trend more clearly: the efficiency keeps increasing in the range of the experimental points with an increase of the parameter γ. The figure shows that, although $\eta \approx 3$–5% is quite high for our devices, it could be increased up to $\approx 8\%$ with the increase of γ up to ≈ 0.13. Figs. 9 and 10 show a reasonable agreement between the experiment and theory, and they also illustrate again the point discussed in the theoretical part of the article: depending on the optimization goal (P or η), one should choose different γ, i.e., RTD oscillators with different parameters.

To put the measured performance of our RTD oscillators into context, Table II shows their comparison with the results reported in the literature. One can see, that the output power of our devices is at a decent level, comparable to other reported devices, although the operating frequency of our oscillators is (intentionally) rather low (≈ 100 GHz). The conversion efficiency of our oscillators is also quite high, 5% efficiency is the highest level reported for RTD oscillators integrated with antennas. A higher value of 14.7% has been reported only for the on-chip RTD oscillators with a microwave-probe coupling at 34 GHz [25].

IV. CONCLUSION

We demonstrate that the maximum output power ($P_{\max}$) of RTD oscillators could be assessed by a very simple equation (13), and $P_{\max}$ is fundamentally limited by the radiation conductance of the antenna and by the RTD voltage swing. The latter

can be approximated as the peak-to-valley voltage separation of the RTD $I-V$ curve. Surprisingly, the RTD current density, its differential conductance, and capacitance have no direct influence on $P_{\max}$. However, those parameters do determine a parameter γ, which defines how close one can come to $P_{\max}$ in an RTD oscillator; the higher the RTD conductance and smaller its capacitance, the smaller is γ and the closer the output power can come to $P_{\max}$. It turns out, the common single-antenna RTD oscillators have rather low radiation conductance to achieve more (or at least significantly more) than 1-mW output power radiated into free space. For the power levels of 1 mW and above, more sophisticated designs of RTD oscillators with more complex antenna concepts or with additional radiator antennas are required. We also show that the maxima of the output power and efficiency of RTD oscillators are not achieved simultaneously, the maxima correspond to different sets of oscillator parameters (different γ).

In the experimental part of the work, we report on symmetrical slot-antenna RTD oscillators operating at the values of the parameter $\gamma \approx 0.05$–0.08, which correspond to a maximum of the output power for the given wafer and given type of the oscillator antenna. In the frequency range of 90–110 GHz, the emitted power was at the level of $\approx$ 380–500 μW. The dc-to-RF conversion efficiency of our oscillators is at the 5% level, which is the highest reported for antenna-coupled RTD oscillators. We show that the efficiency of our oscillators could be increased up to 8%, although at the expense of reduced output power.

ACKNOWLEDGMENT

The authors would like to thank the Center for Micro- and Nanostructures for providing clean-room facilities.

REFERENCES

[1] M. Asada and S. Suzuki, "Room-temperature oscillation of resonant tunneling diodes close to 2 THz and their functions for various applications," *J. Infrared Millimeter Terahertz Waves*, vol. 37, pp. 1185–1198, Dec. 2016.
[2] M. Feiginov, "Frequency limitations of resonant-tunnelling diodes in sub-THz and THz oscillators and detectors," *J. Infrared Millimeter Terahertz Waves*, vol. 40, pp. 365–394, 2019.
[3] R. Izumi, S. Suzuki, and M. Asada, "1.98 THz resonant-tunneling-diode oscillator with reduced conduction loss by thick antenna electrode," in *Proc. IEEE 42nd Int. Conf. Infrared, Millimeter, Terahertz Waves*, 2017, pp. 1–2.
[4] S. Suzuki et al., "RTD oscillators at 430–460 GHz with high output power (200 μW) using integrated offset slot antennas," in *Proc. IEEE 22nd Int. Conf. Indium Phosphide Related Mater.*, 2010, pp. 1–4.
[5] M. Shiraishi et al., "High output power (μw) oscillators at around 550 GHz using resonant tunneling diodes with graded emitter and thin barriers," *Appl. Phys. Exp.*, vol. 4, no. 6, May 2011, Art. no. 064101.
[6] Y. Koyama et al., "A high-power terahertz source over 10 mW at 0.45 THz using an active antenna array with integrated patch antennas and resonant-tunneling diodes," *IEEE Trans. THz Sci. Technol.*, vol. 12, no. 5, pp. 510–519, Sep. 2022.
[7] P. Ourednik, T. Hackl, C. Spudat, D. T. Nguyen, and M. Feiginov, "Double-resonant-tunneling-diode patch-antenna oscillators," *Appl. Phys. Lett.*, vol. 119, no. 26, 2021, Art. no. 263509.
[8] C. Kim and A. Brandli, "High-frequency high-power operation of tunnel diodes," *IRE Trans. Circuit Theory*, vol. 8, no. 4, pp. 416–425, 1961.
[9] M. Asada, S. Suzuki, and N. Kishimoto, "Resonant tunneling diodes for sub-terahertz and terahertz oscillators," *Jap. J. Appl. Phys.*, vol. 47, no. 6, pp. 4375–4384, Jun. 2008.
[10] K. Urayama et al., "Sub-terahertz resonant tunneling diode oscillators integrated with tapered slot antennas for horizontal radiation," *Appl. Phys. Exp.*, vol. 2, 2009, Art. no. 044501.
[11] M. Feiginov, C. Sydlo, O. Cojocari, and P. Meissner, "Resonant-tunnelling-diode oscillators operating at frequencies above 1.1 THz," *Appl. Phys. Lett.*, vol. 99, 2011, Art. no. 233506.
[12] S. Diebold et al., "High-speed error-free wireless data transmission using a terahertz resonant tunnelling diode transmitter and receiver," *Electron. Lett.*, vol. 52, no. 24, pp. 1999–2001, 2016.
[13] K. Kasagi, S. Suzuki, and M. Asada, "Array configuration using resonant-tunneling-diode terahertz oscillator integrated with patch antenna," in *Proc. IEEE 40th Int. Conf. Infrared, Millimeter, Terahertz waves*, 2015, pp. 1–2.
[14] K. Kasagi, S. Suzuki, and M. Asada, "Large-scale array of resonant-tunneling-diode terahertz oscillators for high output power at 1 THz," *J. Appl. Phys.*, vol. 125, no. 15, 2019, Art. no. 151601.
[15] R. Sekiguchi, Y. Koyama, and T. Ouchi, "Subterahertz oscillations from triple-barrier resonant tunneling diodes with integrated patch antennas," *Appl. Phys. Lett.*, vol. 96, 2010, Art. no. 062115.
[16] P. Ourednik and M. Feiginov, "Double-resonant-tunneling-diode bridgeless patch-antenna oscillators operating up to 1.09 THz," *Appl. Phys. Lett.*, vol. 120, no. 18, 2022, Art. no. 183501.
[17] M. N. Feiginov, "Effect of the coulomb interaction on the response time and impedance of the resonant-tunneling diodes," *Appl. Phys. Lett.*, vol. 76, 2000, Art. no. 2904.
[18] M. N. Feiginov, "Does the quasibound-state lifetime restrict the high-frequency operation of resonant-tunnelling diodes?," *Nanotechnology*, vol. 11, 2000, Art. no. 359.
[19] M. N. Feiginov, "Displacement currents and the real part of high-frequency conductance of the resonant-tunneling diode," *Appl. Phys. Lett.*, vol. 78, 2001, Art. no. 3301.
[20] M. Feiginov, H. Kanaya, S. Suzuki, and M. Asada, "Operation of resonant-tunneling diodes with strong back injection from the collector at frequencies up to 1.46 THz," *Appl. Phys. Lett.*, vol. 104, 2014, Art. no. 243509.
[21] M. Feiginov, C. Sydlo, O. Cojocari, and P. Meissner, "High-frequency nonlinear characteristics of resonant-tunnelling diodes," *Appl. Phys. Lett.*, vol. 99, 2011, Art. no. 133501.
[22] M. N. Feiginov and D. R. Chowdhury, "Operation of resonant-tunneling diodes beyond resonant-state-lifetime limit," *Appl. Phys. Lett.*, vol. 91, 2007, Art. no. 203501.
[23] A. Al-Khalidi, K. Alharbi, J. Wang, and E. Wasige, "A compact terahertz source technology for automotive radar and other applications," in *Proc. 19th Int. Radar Symp.*, 2018, pp. 1–6.
[24] F. Han et al., "Impedance matching in high-power resonant-tunneling-diode terahertz oscillators integrated with rectangular-cavity resonator," *IEICE Trans. Electron.*, vol. E104.C, no. 8, pp. 398–402, 2021.
[25] A. C. Cornescu et al., "High-efficiency bias stabilization for resonant tunneling diode oscillators," *IEEE Trans. Microw. Theory Techn.*, vol. 67, no. 8, pp. 3449–3454, Aug. 2019.
[26] M. Feiginov, C. Sydlo, O. Cojocari, and P. Meissner, "Operation of resonant-tunnelling oscillators beyond tunnel lifetime limit," *Europhys. Lett.*, vol. 94, no. 4, May 2011, Art. no. 48007.

Christian Spudat received the M.Sc. degree in physics from Freie Universität Berlin, Berlin, Germany, in 2006, and the Ph.D. degree in physics from Universität Duisburg-Essen, Duisburg, Germany, in 2010.

From 2006 to 2010, he was with Research Center Jülich, Jülich, Germany, as a Research Associate. From 2011 to 2015, he was with the Fraunhofer Institute for Electronic Nano Systems, Chemnitz, Germany, as a Researcher. Since 2016, he has been with Technische Universität Wien, Vienna, Austria, as a Researcher. His research interests include carbon nanostructures and THz electronics.

Petr Ourednik received the B.E. and M.E. degrees in electrical engineering from Czech Technical University, Prague, Czech Republic, in 2014 and 2016, respectively. Since 2018, he has been working toward the Ph.D. degree in electrical engineering with Technische Universität Wien, Vienna, Austria.

From 2016 to 2018, he was Czech Technical University as a Research Associate. His research interests include high-frequency and THz electronics.

Gabriele Picco received the B.Sc. and M.Sc. degrees in physics from Università degli studi di Trieste, Trieste, Italy, in 2016 and 2019, respectively. Since 2021, he has been working toward the Ph.D. degree in electrical engineering with Technische Universität Wien, Vienna, Austria.

His research interests include semiconductor physics and THz electronics.

Dinh Tuan Nguyen received the B.E. and M.E. degrees in electrical engineering from the Moscow Institute of Physics and Technology, Moscow, Russia, in 2010 and 2012, respectively. Since 2018, he has been working toward the Ph.D. degree in electrical engineering with Technische Universität Wien, Vienna, Austria.

From 2013 to 2019, he was with Le Quy Don Technical University, Hanoi, Vietnam, as a Teaching Assistant and a Lecturer. His research interests include THz electronics.

Michael Feiginov received the M.Sc. degree in electrical engineering and physics from the Moscow Institute of Physics and Technology, Moscow, Russia, in 1994, and the Ph.D. degree in physics of semiconductors and dielectrics from the Institute of Radioengineering and Electronics, Russian Academy of Sciences, Moscow, in 1999.

From 1994 to 2000, he was with the Institute of Radioengineering and Electronics, Russian Academy of Sciences, as a Junior Scientist, Scientist, and Senior Scientist. In 2001, he was with Technische Universität Chemnitz, Chemnitz, Germany, as a Researcher. From 2002 to 2013, he was with Technische Universität Darmstadt, Darmstadt, Germany, as a Senior Researcher. From 2013 to 2014, he was with the Tokyo Institute of Technology, Tokyo, Japan, as a Visiting Researcher. From 2014 to 2016, he was with Canon Inc., Tokyo, as a Scientific Manager with Frontier Research Center. Since 2016, he has been a Professor with Technische Universität Wien, Vienna, Austria. His research interests include THz electronics and photonics.